Malaysian Journal of Mathematical Sciences 20(2): 537–558 (2026)
https://doi.org/10.47836/mjms.20.2.05

Malaysian Journal of Mathematical Sciences

Journal homepage: https://mjms.upm.edu.my

Thermosolutal Mixed Convection in Vertical Pipe under Chemical Reaction and Thermal Radiation

Kapoor, S.[1] and Sahoo, S. *[2]

[1]*Department of Education in Science and Mathematics, Regional Institute of Education (NCERT), Bhubaneswar - 751022, Odisha, India*
[2]*Department of Mathematics, Utkal University, Bhubaneswar - 751004, Odisha, India*

E-mail: siprarani_rs@utkaluniversity.ac.in
**Corresponding author*

Received: 9 April 2025
Accepted: 30 September 2025

Abstract

The present study numerically investigates the influence of thermal radiation and chemical reaction on thermosolutal mixed convection in a vertical pipe embedded in a porous medium, focusing on air water systems, which are directly applicable in technologies such as humidification-dehumidification desalination units and industrial cooling towers. The flow dynamics are modeled using the non Darcy Brinkman Forchheimer (NDBF) extended framework. The flow is driven by a combination of buoyancy forces arising from temperature and solute concentration gradients, along with an external pressure gradient. The governing coupled differential equations are solved using the Chebyshev spectral collocation method for high accuracy and spectral convergence. The results demonstrate that both the thermal radiation parameter (R) and chemical reaction parameter (γ) significantly affect the velocity, temperature, and concentration profile of an air-water system. According to our findings, 'R' has a substantial effect on the instability of the fluid flow mechanism. In a Darcy porous media, where the Darcy number ranges from 10^{-5} to 10^{-2}, the Prandtl number is taken as $\mathrm{Pr} = 0.71$ for air and is $\mathrm{Pr} = 7$ for water, it has been observed that the point of inflection arises faster in radiative flow than in non radiative flow with change of radiation parameter from 1 to 3 and subsequently to 5. The radiation parameter (R) leads to a decrease in temperature profile due to enhanced radiative heat loss, while it causes an increase in concentration profile. Additionally, as the chemical reaction parameter increases, the concentration profile diminishes due to species consumption. A similar suppressive effect on concentration is observed with higher Schmidt number (Sc), which indicates reduced mass diffusivity.

Keywords: thermosolutal mixed convection; porous medium; pipe flow; thermal radiation; chemical reaction; spectral collocation method.

1 Introduction

Heat and mass transfer in porous media is essential in various engineering and natural systems, including chemical reactors, geothermal energy, heat exchangers, and biological transport. When both temperature and concentration gradients are present, thermosolutal (double-diffusive) convection arises, leading to complex flow and transport behaviors. Thermal energy transfer plays a vital role in many industrial and technological systems to manage heat and prevent overheating. Heat is transferred through three primary mechanisms: conduction, convection, and radiation. Conduction involves heat flow through direct contact, while convection is driven by the bulk movement of fluid. Thermal radiation, the transfer of energy via electromagnetic waves, becomes significant in high temperature environments. In thermal analyses of modern engineering systems, radiation effects must often be considered especially when it dominates or interacts with other modes of heat transfer. Thermal radiation analysis is crucial in various applications, including aerospace systems, high-temperature processes, power generation, and solar energy. In medical science, it also plays a key role in treatments like thermal therapy for cancerous tissues [12].

Radiation and convection are interdependent heat transfer modes, both influenced by temperature dependent properties. When radiation is significant, it must be coupled with convection due to their nonlinear interaction, making the combined problem complex to solve. Chiou [7] investigated the combined effects of radiation and convection heat transfer in pipes under reflood steam cooling conditions, highlighting the role of radiation in high-temperature steam flows. Building on this, Yang [35] examined mixed convection with thermal radiation in a vertical pipe, demonstrating the influence of radiative parameters and buoyancy forces on the local Nusselt number and velocity distribution. Also, Yang [36] conducted a numerical study on forced convection in vertical pipe flow, incorporating both radiation and buoyancy effects. His findings revealed that radiation enhances heat transfer by reducing the temperature gradient across the pipe, thereby diminishing density variations and weakening the buoyancy-driven flow. Furthermore, Campo and Schuler [6, 30] developed a radiation transport model using the moment method and numerically solved the coupled heat transfer problem. Their work addressed both laminar and turbulent forced convection with thermal radiation in the thermal entrance region of an isothermal pipe, providing valuable insights into radiative-convective interactions in pipe flow. Continuing in this direction, thermal radiation effect in pipe flow, Ahmad et al. [1] also invesigated that by considering one-dimensional Eyring-Powell fluid. Their findings show the temperature profile predicts the declining behavior of the radiation parameter.

Many science and engineering sectors benefit from chemical reaction mass transfer research. This type of flow has several industrial and engineering applications including nuclear reactor, metallurgy, in chemical engineering and combustion systems. Most of industrial chemical processes are converting the cheaper raw materials into high-valued products, commonly through chemical reactions. Bachok et al. [4] studies on homogeneous-heterogeneous reactions near the stagnation point of a stretching surface revealed that reaction parameters control boundary layer behavior. Furthermore, an analytical investigation on solute dispersion in peristaltic flow considering combined homogeneous and heterogeneous chemical reactions was conducted by Sankad and Dhange [29]. Similarly, a study on steady MHD flow of a non-Newtonian power-law fluid over a continuously moving stretching surface with chemical reaction has been analyzed by Hayat et al. [9], the influence of magnetic and reaction parameters on the flow and mass transfer behavior has been demonstrated. Furthermore, a numerical investigation on non-Newtonian fluid under chemical reaction over a radiative paraboloid surface was presented by Sobhana et al. [31], while Sridhar et al. [32] conducted a computational study on micropolar fluid flow over a stretched surface with chemical reaction. Noon [19] examined the impact of chemical reactions on rotating thermosolutal mixed convection, highlighting that chemical reactions, rotation, and variations in gravity significantly affect the onset of convection and the critical Rayleigh number in Darcy porous media. Considering the importance of chemical reactions in pipe flow analysis is evidented from studies in [20, 8]. Ooms et al. [20] developed a model for turbulent heat transfer in pipe flow involving a first-order chemical reaction, demonstrating its notable impact on flow dynamics and thermal behavior. Similarly, Chitra and Kavitha [8] investigated MHD flow in a porous vertical pipe and observed that increasing the chemical reaction parameter leads to a decline in concentration levels.

Chemical-thermal radiation interactions in fluid flow is crucial for optimizing various engineering processes. Understanding this interaction can lead to improved system performance and energy efficiency in applications such as high temperature chemical reactors, like combustion chambers and reformers, often use vertical porous systems where radiation dominates heat transfer, significantly affecting reaction rates. Other applications include solar energy receivers, thermal collectors, waste heat recovery systems, catalytic reactors, and biomedical systems involving drug perfusion in porous tissues, where controlled chemical reactions and thermal radiation respond to local temperature and concentration gradients. Matao et al. [17] conducted an investigation on the effects of Hall current and viscous dissipation in a mixed convection MHD fluid flow past a vertical porous plate, incorporating both chemical reactions and thermal radiation. Extending this, Reddy et al. [26, 27] performed numerical simulations on Casson MHD fluids under similar conditions, highlighting the interplay of chemical reactivity and radiative heat transfer in vertical porous systems. Additionally, a finite difference approach was adopted by Reddy et al. [28] to examine the combined impact of thermodiffusion (Soret effect) and chemical reactions on radiative MHD flow through porous plates. Further studies by the same group [24, 25] explored thermodiffusion and unsteady mixed convection in MHD Casson fluids, emphasizing the significant role of thermal radiation and chemical reaction. Recent studies have numerically investigated MHD Casson nanofluid flows in different configurations. Madhavi et al. [16] analyzed heat source effects over a porous wedge for electrically conducting Casson nanofluids with activation energy, including second-law analysis and chemical reactions. Similarly, Rani et al. [21] explored hybrid Casson nanofluid stagnation-point flow over a transient stretching surface under thermal radiation and Joule heating.

Hayat et al. [10] examined 3D MHD flow with thermal radiation and chemical reactions, showing that increased radiation raises temperature but reduces concentration, while the chemical reaction parameter similarly lowers concentration. Arifuzzaman et al. [3] studied MHD Maxwell fluid on a vertical porous plate, observing that radiation enhances temperature and velocity, whereas higher-order reactions reduce concentration. Contrarily, Reddy [23] reported that radiation decreases both temperature and velocity in mixed convective MHD flow. Akter et al. [2] explored thermodiffusion and chemical reaction effects, noting that higher Prandtl numbers reduce velocity and temperature, and increased reaction parameters reduce velocity and concentration. Recently, Yedhiri et al. [37] analyzed nonlinear mixed convective MHD flow in a porous channel with radiation and chemical reaction, further affirming the significance of these parameters in modulating flow and transport properties.

Considering vertical pipe flows in porous media, which have been studied by many researchers due to their relevance in vertical heat exchangers, reactive porous columns, and geothermal boreholes. In such configurations, fluid flow is often driven by an external pressure gradient and buoyancy forces caused by temperature and concentration differences. Previous studies, such as Kumar et al. [15] investigated the mechanism of double diffusive mixed convective fluid flow considered in a vertical pipe. Bera et al. [5] study double diffusive mixed convection under local thermal non equilibrium in vertical pipe. Kapoor et al. [11] numerically investigate the impact of Rayleigh number on non-Darcy thermosolutal mixed convective flow in a vertical pipe. However, these works often simplify the system by ignoring radiation effects, neglecting chemical reactions, which limits their application to real-world scenarios. The present study aims to develop a more comprehensive model by incorporating the non-Darcy Brinkman-Forchheimer (NDBF) model, thermal radiation (via the Rosseland approximation), and first-order chemical reaction into the formulation of mixed thermosolutal convection in a vertical porous pipe. The pipe wall is assumed to have linearly varying temperature and concentration, and the pipe is embedded in a homogeneous and isotropic porous medium. The considered specified boundary conditions simulate a fully developed, axisymmetric thermosolutal flow through a vertical pipe, commonly encountered in engineering, geophysical, and industrial piping system.

2 Mathematical Formulation

A thermosolutal mixed convective flow is investigated within a vertical pipe filled with porous medium under thermal radiation and chemical reaction effect. The fluid is considered to be newtonian, incompressible, fully developed and the flow is driven by an external pressure gradient and two buoyancy forces due to temperature and concentration differences. The gravitational force is acting in negative $\tilde{z}$ direction, as shown in the Figure 1.

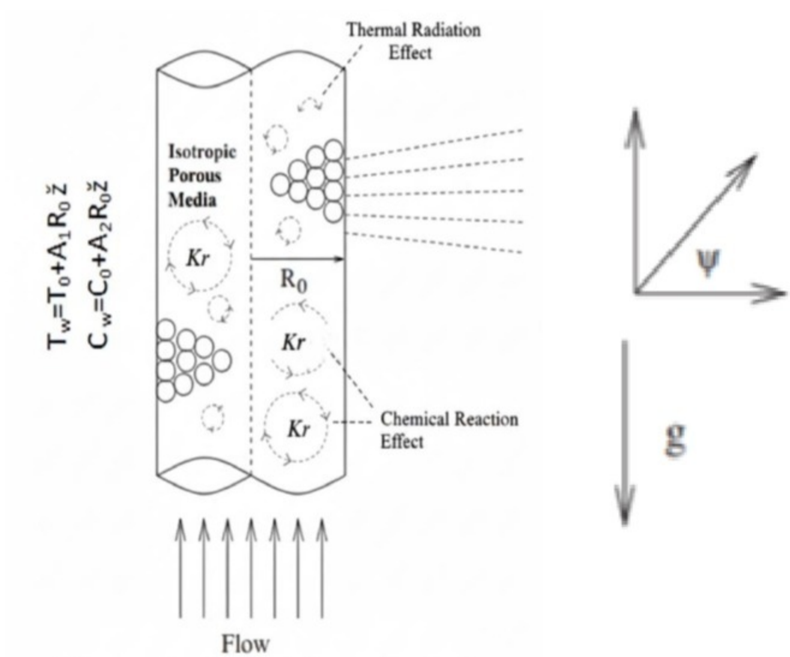

Figure 1: Schematic diagram for vertical flow in pipe.

The wall temperature and solute concentration are prescribed to vary linearly with the vertical coordinate $\tilde{z}$, representing a situation where the pipe wall is subjected to uniform thermal and solutal fluxes. Mathematically, this is expressed as,

$$T_w = T_0 + A_1 R_0 \tilde{z}, \qquad\qquad C_w = C_0 + A_2 R_0 \tilde{z},$$

where A_1 and A_2 are constants, T_0 and C_0 the up stream wall temperature and concentration of the fluid are respectively and R_0 is the radius of pipe.

We consider the non-Darcy Brinkiman-Forchheimer (NDBF) extended model to represent the complex behavior of fluid flow through a porous medium inside a vertical pipe [15, 5]. The pipe is filled with a porous medium of uniform and isotropic permeability, offering equal resistance to flow in all directions. In addition, thermal radiation [18] and chemical reactions [23] are incorporated into the model to simulate high-temperature reactive flows, which are common in chemical reactors, geothermal systems, and industrial heat exchangers. The flow is steady, fully developed, and unidirectional, with velocity vector of $(0, 0, \tilde{w})$, implying motion only in the axial direction. Based on these assumptions, the governing equations for continuity, momentum (incorporating the NDBF model), energy under thermal radiation, and species transport with chemical reaction are expressed in cylindrical coordinates.

Continuity equation:

$$\frac{\partial \tilde{w}}{\partial \tilde{z}} = 0. \tag{1}$$

Momentum equation:

$$\begin{aligned} \rho_f \left[\frac{1}{\epsilon} \frac{\partial \tilde{w}}{\partial \tilde{t}} + \frac{1}{\epsilon^2} \left(\tilde{J} \tilde{w} \right) + \frac{c_F}{K^{\frac{1}{2}}} \left(\sqrt{\tilde{u}^2 + \tilde{v}^2 + \tilde{w}^2} \right) \tilde{w} \right] = \\ - \frac{\partial \tilde{p}}{\partial \tilde{z}} + \mu' \left[\tilde{D}^2 \tilde{w} \right] - \mu_f \frac{\tilde{w}}{K} + \rho_f g \left[\beta_T \left(\tilde{T} - T_w \right) + \beta_C \left(\tilde{C} - C_w \right) \right]. \end{aligned} \tag{2}$$

Energy equation:

$$\sigma \frac{\partial \tilde{T}}{\partial \tilde{t}} + \left[\tilde{J} \tilde{T} \right] = \alpha_e \left[\tilde{D}^2 \tilde{T} \right] - \frac{1}{C_p} \frac{\partial q_r}{\partial r}. \tag{3}$$

Solutal equation:

$$\epsilon \frac{\partial \tilde{C}}{\partial \tilde{t}} + \left[\tilde{J} \tilde{C} \right] = \bar{D} \left[\tilde{D}^2 \tilde{C} \right] - k_r \tilde{C}, \tag{4}$$

whereby,

$$\tilde{J} = \tilde{u} \frac{\partial}{\partial \tilde{r}} + \frac{\tilde{v}}{\tilde{r}} \frac{\partial}{\partial \psi} + \tilde{w} \frac{\partial}{\partial \tilde{z}}, \qquad \text{and} \qquad \tilde{D}^2 = \frac{\partial^2}{\partial \tilde{r}^2} + \frac{1}{\tilde{r}} \frac{\partial}{\partial \tilde{r}} + \frac{1}{\tilde{r}^2} \frac{\partial^2}{\partial \psi^2} + \frac{\partial^2}{\partial \tilde{z}^2}.$$

Here,

$(\tilde{u}, \tilde{v}, \tilde{w})$: flow velocity components,
K : permeability of the porous medium,
$\tilde{T}$: temperature,
$\tilde{C}$: concentration of solute,
μ_f : fluid velocity,
g : gravitational acceleration,
ρ_f : reference-state fluid density,
β_C : solutal volume expansion coefficient,
β_T : volumetric thermal expansion,
$\tilde{p}$: pressure,
$\tilde{t}$: time,
$\bar{D}$: solute diffusivity,
α_e : thermal diffusivity,
μ' : effective viscosity,
ϵ : porosity of the medium,
$\sigma = \frac{(\rho c_s)_m}{(\rho c_p)_f}$: heat capacities ratio,
k_r : chemical reaction rate,

The radiative heat flux for thermal radiation (q_r), in Rosseland approximation is presented by [22],

$$q_r = -\frac{4\sigma_1}{3k_1}\frac{\partial T^4}{\partial r}.$$

Hereby, σ is the Stefan-Boltzmann constant, and k_1 is the average absorption coefficient. Flow temperature variations are represented by T^4 being a function of temperature. To do this, ignore higher-order terms and extend T^4 in the Taylor series of T_0,

$$T^4 = {T_0}^4 + (T - T_0)4{T_0}^3 + \frac{(T - T_0)^2}{2!}12{T_0}^2 \cdots = 4T{T_0}^3 - 3{T_0}^4.$$

By using the non-dimensional quantities listed below,

$$r = \frac{\tilde{r}}{R_0}, \qquad u = \frac{\tilde{u}}{\tilde{W}_c}, \qquad v = \frac{\tilde{v}}{\tilde{W}_c}, \qquad w = \frac{\tilde{w}}{\tilde{W}_c}, \qquad z = \frac{\tilde{z}}{R_0},$$
$$p = \frac{\tilde{p}}{\rho_f {\tilde{W}_c}^2}, \qquad t = \frac{t^8 \tilde{W}_c}{R_0}, \qquad \theta = \frac{T_w - \tilde{T}}{A_1 {R_0}^2 RePr}, \qquad \Phi = \frac{C_w - \tilde{C}}{A_2 {R_0}^2 ReSc},$$

the governing differential equations (1)–(4) are

$$\frac{\partial w}{\partial z} = 0, \tag{5}$$

$$\left[\frac{1}{\epsilon}\frac{\partial w}{\partial t} + \frac{1}{\epsilon^2}(Jw)\right] + F\left(\sqrt{u^2 + v^2 + W^2}\right)w = -\frac{\partial p}{\partial z} + \frac{1}{Re}\left[D^2 w\right] - \frac{\Delta}{ReDa}w - \frac{(Ra_T\theta + Ra_s\Phi)}{Re}, \tag{6}$$

$$\sigma\frac{\partial \theta}{\partial t} + [J\theta] = \frac{1}{RePr}w + \frac{1}{RePr}\left[D^2\theta\right] + \frac{1}{RePr}R\frac{\partial^2\theta}{\partial r^2}, \tag{7}$$

$$\epsilon\frac{\partial \Phi}{\partial t} + [J\Phi] = \frac{1}{ReSc}w + \frac{1}{ReSc}\left[D^2\Phi\right] - \frac{\gamma\Phi Sc}{ReSc} + \frac{k_a}{ReSc}, \tag{8}$$

whereby,

$$J = u\frac{\partial}{\partial r} + \frac{v}{r}\frac{\partial}{\partial \psi} + w\frac{\partial}{\partial z}, \qquad \text{and} \qquad D^2 = \frac{\partial^2}{\partial r^2} + \frac{1}{r}\frac{\partial}{\partial r} + \frac{1}{r^2}\frac{\partial^2}{\partial \psi^2} + \frac{\partial^2}{\partial z^2}.$$

The above equations use dimensionless parameters (u, v, w) as non-dimensional velocity vector of the fluid, θ as temperature of fluid, Φ as concentration of fluid, p is pressure and t is temperature. Another non-dimensional parameters considered are:

Rayleigh thermal number, $Ra_T = \dfrac{g\beta_T A_1 {R_0}^5}{\tilde{v}\alpha}$, Reynold number, $\mathrm{Re} = \dfrac{W_c^* R_0}{\tilde{v}}$,

Rayleigh solutal number, $Ra_s = \dfrac{g\beta_C A_2 {R_0}^5}{\tilde{v}\bar{D}}$, Prandel number, $\mathrm{Pr} = \dfrac{\tilde{v}}{\alpha_e}$,

Schmidt number, $\mathrm{Sc} = \dfrac{\tilde{v}}{\bar{D}}$, Darcy number, $\mathrm{Da} = \dfrac{K}{R_0^2}$,

Forchheimer number, $\mathrm{F} = \dfrac{R_0 {W_c^*}^2 c_F}{k^{\frac{1}{2}}}$, buoyancy ratio, $N = \dfrac{Ra_s}{Ra_T}$,

viscosity ratio, $\Delta = \dfrac{\mu_f}{\mu}$.

Furthermore,

W_c^* is base velocity at center of the pipe,

$\tilde{v}$ is the kinematic of viscosity, α_e is thermal diffusivity,

$R = \dfrac{16\sigma_1 {T_0}^3}{3\mu C_p k_1}$ is the thermal radiation parameter,

$\gamma = \dfrac{K_r {R_0}^2}{v}$ is the chemical reaction parameter,

$k_a = \dfrac{K_r C_w}{A_2 R_0 {W_c}^*}$.

2.1 Basic flow

Fully developed, stable, unidirectional, laminar flow is basic. Thus, the flow is considered along vertical direction only. Under the above above assumption the preceding governing equations (5)–(8) can be expressed as,

$$\frac{d^2W_0}{dr^2} + \frac{1}{r}\frac{dW_0}{dr} - \frac{\Delta}{Da}W_0 - (Ra_T\Theta_0 + Ra_s\Phi_0) - Re\frac{dp_0}{dz} - ReF|W_0|W_0 = 0, \tag{9}$$

$$\left(\frac{1}{Pr} + R\right)\frac{d^2\Theta_0}{dr^2} + \frac{1}{r}\frac{d\Theta_0}{dr} = -W_0, \tag{10}$$

$$\frac{d^2\Phi_0}{dr} + \frac{1}{r}\frac{d\Phi_0}{dr} - \gamma Sc\Phi_0 + K_a = -W_0. \tag{11}$$

Thus, the boundary conditions are

$$\frac{dW_0}{dr} = \frac{d\Theta_0}{dr} = \frac{d\Phi_0}{dr} = 0, \quad \text{at } r = 0, \tag{12}$$

$$W_0 = \Theta_0 = \Phi_0 = 0, \quad \text{at } r = 1, \tag{13}$$

with W_0, Θ_0, Φ_0 and P_0 representing basic velocity, temperature, concentration, and pressure.

3 Numerical Solution of Basic Flow

Here we calculate numerically the basic flow by dividing (9)–(13) by $Re\dfrac{dp_0}{dz}$. Consequently, the aforementioned equations are adjusted

$$\frac{d^2W}{dr^2} + \frac{1}{r}\frac{dW}{dr} - \frac{1}{Da}W - (Ra_T\Theta + Ra_s\Phi) - 1 - F'|W|W = 0, \tag{14}$$

$$\left(\frac{1}{Pr} + R\right)\frac{d^2\Theta}{dr^2} + \frac{1}{r}\frac{d\Theta}{dr} = -W, \tag{15}$$

$$\frac{d^2\Phi}{dr^2} + \frac{1}{r}\frac{d\Phi}{dr} - \gamma Sc\Phi + k_a = -W. \tag{16}$$

To estimate variables W, Θ, and Φ using Chebyshev polynomials [34], the function $\xi = 1 - 2r$ transforms the independent variable r from the range $[0, 1]$ to $[-1, 1]$.

In terms of ξ, these equations characterize the flow dynamics (14)–(16) with boundary conditions.

Chebyshev variable;

$$-F'|W|W-1+\left(4\frac{d^2W}{d\xi^2}-\frac{4}{1-\xi}\frac{dW}{d\xi}\right)-\frac{1}{Da}W-(Ra_T\Theta+Ra_s\Phi)=0, \tag{17}$$

$$\left(\frac{1}{Pr}+R\right)4\frac{d^2\Theta}{d\xi^2}-\frac{4}{1-\xi}\frac{d\Theta}{d\xi}=-W, \tag{18}$$

$$4\frac{d^2\Phi}{d\xi^2}-\frac{4}{1-\xi}\frac{d\Phi}{d\xi}-\gamma Sc\Phi+k_a=-W, \tag{19}$$

subject to boundary conditions:

$$W=\Theta=\Phi=0,\ \text{ at }\ \xi=1, \qquad \text{and} \qquad \frac{dW}{d\xi}=\frac{d\Theta}{d\xi}=\frac{d\Phi}{d\xi}=0,\ \text{ at }\ \xi=1.$$

For Chebyshev variable ξ, discretized governing equations are (17)–(19)

$$-F|W|W_j+4\sum_{k=0}^{M}B_{jk}W_k-\left(\frac{4}{1-\xi_i}\right)\sum_{k=0}^{M}A_{jk}W_k-\frac{1}{Da}W_j-(Ra_T\Theta_j+Ra_s\Phi_j)=1, \tag{20}$$

$$W_j+\left(\frac{1}{Pr}+R\right)4\sum_{k=0}^{M}B_{jk}\Theta_k-\left(\frac{4}{1-\xi_i}\right)\sum_{k=0}^{M}A_{jk}\Theta_k=0, \tag{21}$$

$$(W_j+k_a)+4\sum_{k=0}^{M}B_{jk}\Phi_k-\left(\frac{4}{1-\xi_i}\right)\sum_{k=0}^{M}A_{jk}\Phi_k-\gamma sc\Phi_k=0, \tag{22}$$

where $j=1,2,3,\dots,M-1$.

The corresponding boundary conditions are

$$W_j=\Theta_j=\Phi_j=0, \qquad \text{at} \quad \xi=-1, \tag{23}$$

and

$$\sum_{k=0}^{M}A_{jk}W_k=\sum_{k=0}^{M}A_{jk}\Theta=\sum_{k=0}^{M}A_{jk}\Phi=0, \qquad \text{at}\ \ \xi=1, \tag{24}$$

where $j=0$ and M.

In the above equations,

$$A_{jk}=\begin{cases}\dfrac{c_j(-1)^k+j}{c_k(\xi_j-\xi_k)}, & j\neq k,\\[2ex] \dfrac{2M^2+1}{6}, & j=k=0,\\[2ex] -\dfrac{2M^2+1}{6}, & j=k=M,\\[2ex] \dfrac{\xi_j}{2(1-\xi_j^2)}, & 1\leq j=k\leq M-1,\end{cases}$$

and $B_{jk} = A_{jm}.A_{mk}$.

In the above,

$$c_j = \begin{cases} 1, & 1 \leq j \leq M-1, \\ 2, & j = 0, M, \end{cases}$$

and $\xi_j = \cos\left(\frac{\pi j}{M}\right)$, where $0 \leq j \leq M$ are considered Chebyshev collocation points and M is the order of polynomial. Subject to boundary conditions, the aforementioned equations yield the following system,

$$AX = b. \tag{25}$$

The square matrix A is a obtained from the discritized differential operators of left hand side of (20)–(24), b is the column matrix obtained from right hand sides of (20)–(24) and X is the column matrix of unknown field variables. The matrices A, X and b having orders are $(3M+3)\times(3M+3)$, $(3M+3)\times 1$ and $(3M+3)\times 1$, accordingly. The linear equation system (25) was solved using MATLAB's A/b tool.

To obtain basic velocity, temperature and concentration,

$$W_0 = \left(Re\frac{dp_0}{dz}\right)W, \quad \Theta_0 = \left(Re\frac{dp_0}{dz}\right)\Theta, \quad \text{and} \quad \Phi_0 = \left(Re\frac{dp_0}{dz}\right)\Phi.$$

For $Re\frac{dp_0}{dz}$, the axial pressure gradient is calculated using global mass conservation,

$$\int_0^1 r\left(Re\frac{dp_0}{dz}\right)W(r)dr = \frac{1}{2}.$$

This implies,

$$\left(Re\frac{dp_0}{dz}\right) = \frac{1}{2\int_0^1 rW(r)dr}.$$

4 Results and Discussion

To gain deeper insight into the physics of thermosolutal mixed convection fluid flow in a vertical pipe through a porous medium under the influence of heat radiation and chemical reactions, we computed numerical results and to demonstrate results of the given analysis for various dynamical parameters involved in the topic under consideration. The behavior of velocity profile, temperature profile, and concentration profile can be seen in plotted Figures 2 to 17. The considered fluids for the study are air having Pr $= 0.71$ and water having Pr $= 0.7$ at 20° and the corresponding Schmidt number (Sc) value is taken as 0.60 which is the same as water vapor and is a chemical species that diffuses through air that is most often studied [23]. The other parameters such as Ra_T (Thermal Rayleigh number), Ra_s (Solutal Rayleigh number), F (Forchheimer number) are fixed at 1000, 500 and 1 respectively as per the existing literature sources. Determination of the range for other governing parameters is based on the practical applications of this type of problem. In this study, we have considered four distnict values $(10^{-2}, 10^{-3}, 10^{-4}, 10^{-5})$ of Darcy number, radiation parameter(R) in a range of 0 to 5 and chemical reaction parameter γ in a range between 0 to 3 based on the available literature.

4.1 Code validation of numerical solution

To authenticate the findings provided in the document, we undertook the following processes. The solution's response to grid size was first examined by altering the order of Chebyshev polynomials. Secondly, comparison of the numerical findings with the referenced ones.

By examining Table 1, it illustrates the grid independence characteristics of the obtained numerical results concerning the order of the approximation polynomial, in which basic velocity (W_0), temperature (θ_0) and concentration (Φ_0) are computed by considering different order Chebyshev polynomials varying from 50 to 100 at $r = 0$, at F $= 1$, $Da = 10^{-2}$, $Ra_T = 10^3$, $Ra_s = 500$, Pr $= 0.71$, $R = 1$, $\gamma = 1$, Sc $= 0.60$. It has been observed that the accuracy in velocity and temperature are reached up to 7-digits and in concentration up to 6 digits. In Table 2, we have compared our present work with the previous results [5] at $Da = 10^{-2}$, $Ra_T = 10^3$, F $= 0$, $R = \gamma = 0$ at different buoyancy ratio (N). The new findings closely align with the previous ones when γ and R are taken to be zero.

Table 1: At $r = 0$ dependence of the velocity, temperature and concentration of the flow on the order of approximation polynomial at Pr $= 0.71$, F $= 1$, $Ra_T = 10^3$, $Ra_s = 500$, Da$= 10^{-2}$, $R = 1$,$\gamma = 1$, Sc $= 0.60$.

N (Terms)	Velocity (W) at $r = 0$	Temperature (θ) at $r = 0$	Concentration (Φ) at $r = 0$
N $= 50$	0.00479580706146543	0.0331092089734551	-0.01373350098986
N $= 55$	0.00479580915376632	0.0331092091334899	-0.01373350134507
N $= 60$	0.00479581041661157	0.0331092107878656	-0.01373350158788
N $= 65$	0.00479581121715774	0.0331092109856344	-0.01373350467882
N $= 70$	0.00479581185249973	0.0331092116705398	-0.01373350644456
N $= 75$	0.00479581225815310	0.0331092125576898	-0.01373350886519
N $= 80$	0.00479581254849595	0.0331092129890078	-0.01373350986733
N $= 85$	0.00479581276085680	0.0331092145450001	-0.01373351166321
N $= 90$	0.00479581276085680	0.0331092186789001	-0.01373351177689
N $= 95$	0.00479581291896386	0.0331092190067583	-0.01373351298001
N $= 100$	0.00479581303870138	0.0331092200089651	-0.01373351452231

Table 2: Comparison with published result [5] and present result at $Da = 10^{-2}$, $Ra_T = 10^3$, F=0, $R = \gamma = 0$.

Buoyancy Ratio (N)	Velocity (W)		Temperature (θ)		Concentration (Φ)	
	Bera et al. [5]	Present work	Bera et al. [5]	Present work	Bera et al. [5]	Present work
0	0.2507699342	0.2507661108	0.1105627481	0.1105879170	0.1072458657	0.1072453233
1	0.1114379510	0.1114370986	0.0902378930	0.0902354648	0.0875307562	0.0875316895
10	-0.0063132885	-0.0063137894	0.0473089399	0.0473086503	0.0458896717	0.0458885469
100	-0.0000950235	-0.0000951378	0.0229862681	0.0229864339	0.0222966800	0.0222966902

4.2 Velocity profile

Figures 2–5 depict the effect of thermal radiation on velocity profile for Darcy values 10^{-2}, 10^{-3}, 10^{-4} and 10^{-5} respectively in a porous vertical pipe flow, with air as the working fluid

(Pr $= 0.71$ and Sc $= 0.60$) and with chemical reaction parameter $\gamma = 1$. Both radiative and non-radiative scenarios are presented for comparison.The results reveal a non-monotonic response of velocity to increasing radiation parameter R. Initially, velocity increases with radiation, due to the enhanced thermal energy available in the system, which boosts buoyancy-driven flow. However, beyond a critical value of R, the velocity begins to decline. This reversal occurs because excessive radiative heat transfer smooths the temperature gradient, thereby weakening the buoyancy force responsible for driving the flow. A distinctive feature observed is the appearance of inflection points in the velocity profiles, which shift closer to the wall as the Darcy number decreases. A lower Darcy number signifies increased porous resistance, which disturbs the balance among pressure, viscous, and buoyancy forces. As a result, the velocity profile's inflection point shifts toward the wall, indicating flow instability. Moreover, radiative cases exhibit inflection points earlier than non-radiative ones, highlighting the destabilizing role of thermal radiation. Radiation modifies the internal energy distribution, which in turn affects both thermal stratification and momentum diffusion, leading to significant changes in flow structure.

Effect of thermal radiation parameter (R) on the velocity profile where the horizontal axis denotes the radial position (r), while the vertical axis corresponds to the velocity component (W_0).

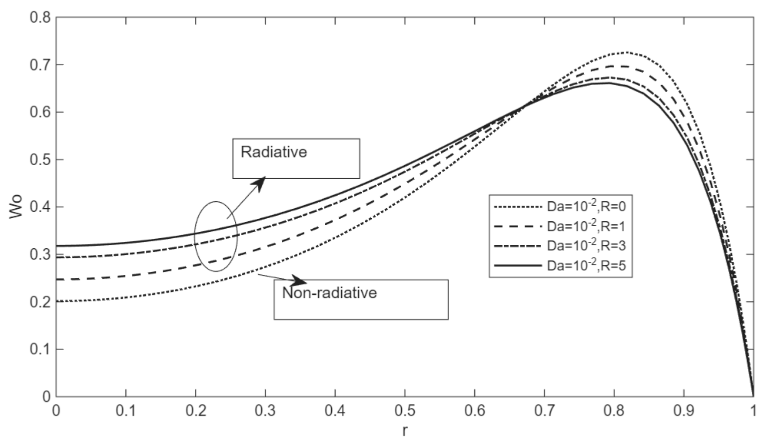

Figure 2: Velocity profile for $Da = 10^{-2}$.

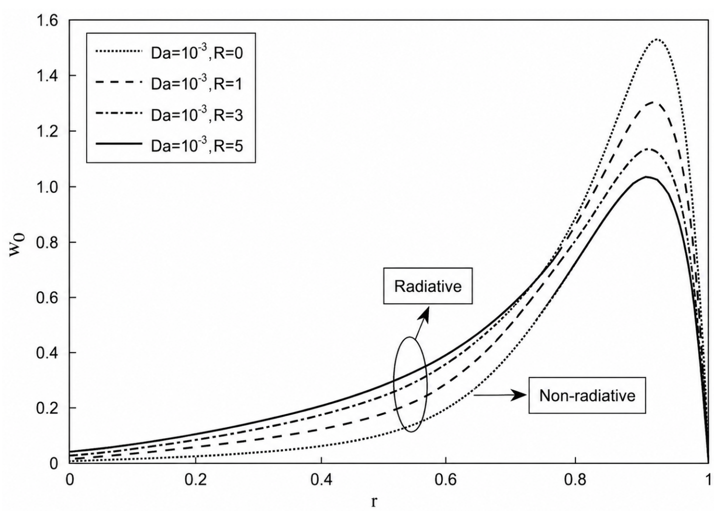

Figure 3: Velocity profile for $Da = 10^{-3}$.

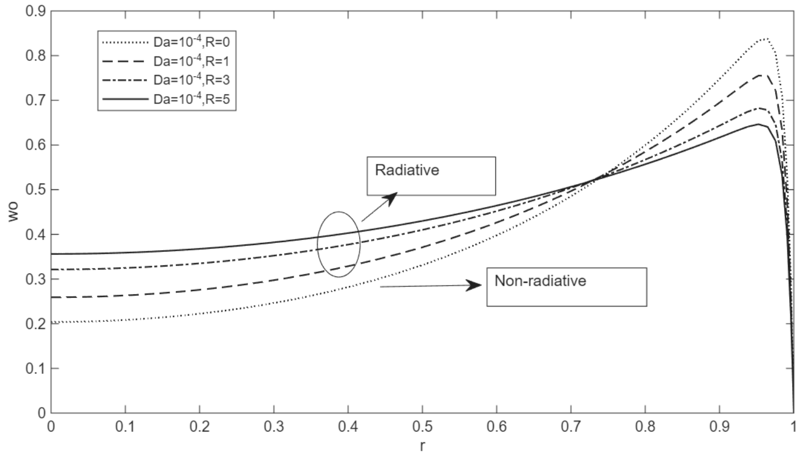

Figure 4: Velocity profile for $Da = 10^{-4}$.

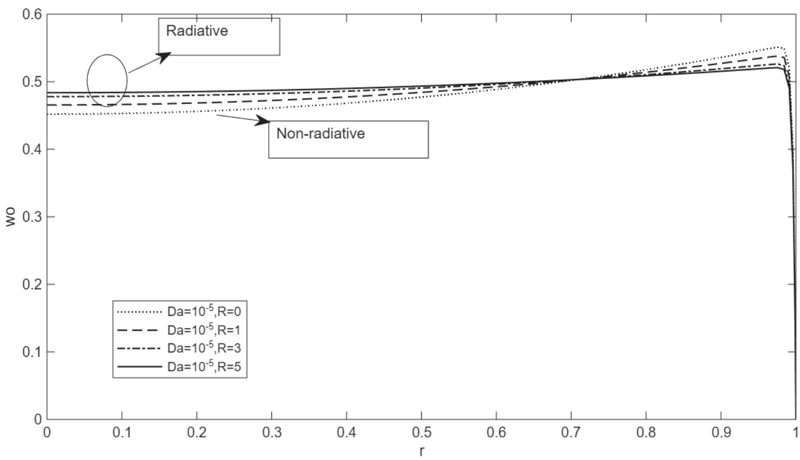

Figure 5: Velocity profile for $Da = 10^{-5}$.

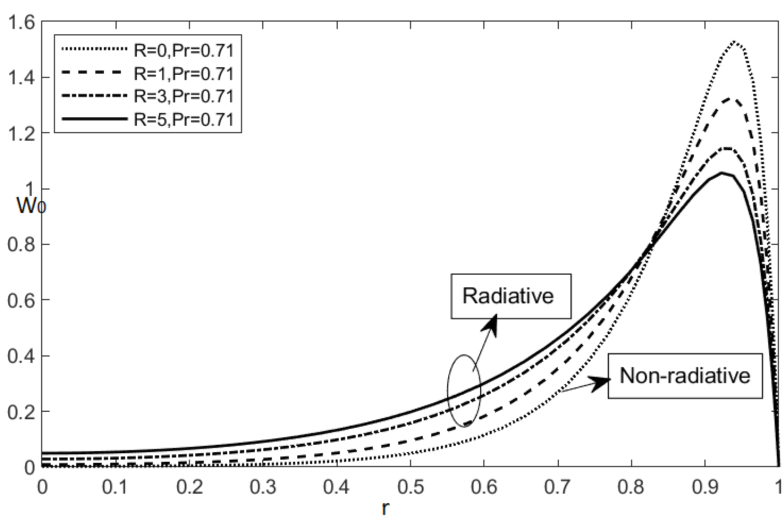

Figure 6: Velocity profile for $Pr = 0.71$.

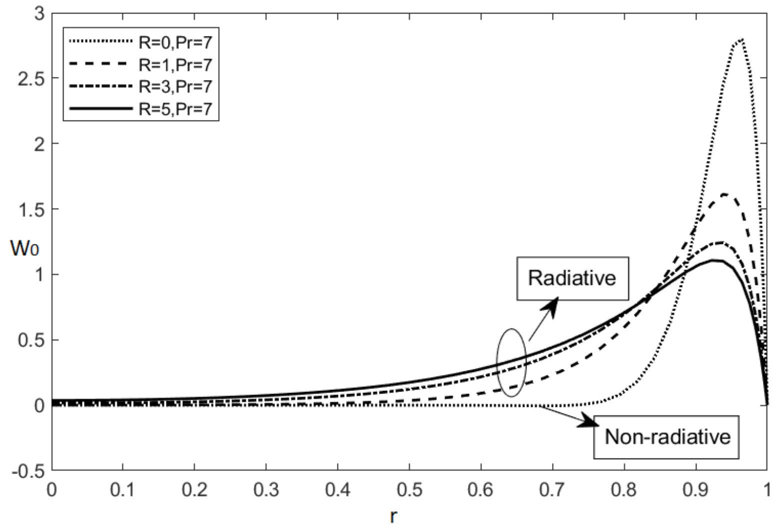

Figure 7: Velocity profile for $Pr = 7$.

Figures 6 and 7 illustrate the influence of thermal radiation on the velocity profile for two different fluids: air Pr $= 0.71$ and water Pr $= 7$, by taking Darcy value $Da = 10^{-3}$. It is observed that with a rise in radiation parameter(R) 1 to 3 and subsequently to 5, the velocity decreases. This behavior aligns with the findings reported in [23]. Another important observation is that the inflection point in the velocity profile appears sooner for water than for air. This is attributed to the higher Prandtl number of water, which implies lower thermal diffusivity. As a result, thermal energy diffuses more slowly in water, maintaining steeper temperature gradients near the wall. This leads to stronger velocity shear and an earlier development of inflection points, signaling a higher tendency toward flow instability compared to air.

4.3 Temperature profile

The impact of R on temperature distribution for Darcy value 10^{-3} and 10^{-5} are plotted in Figures 8 and 9. Both the radiative and non-radiative case well explained, with a rise in thermal radiation parameter(R), from 1 to 3 and subsequently to 5 temperature profile falls accordingly. The figures show that the temperature is highest in the center and falls as one moves towards the pipe's walls. Thermal radiation parameter(R) has a diminishing influence on temperature profile, this trend agrees with previous findings in [1, 23]. The temperature is seen to peak at the pipe center and gradually decrease toward the walls, indicating a typical thermal boundary layer behavior in vertical pipe flows. Physically, an increase in R signifies stronger radiative energy transport, which competes with conduction and convection. Since radiation allows heat to escape more efficiently from the fluid to the surroundings, the internal energy available for conduction and convective heating decreases, leading to cooler temperature profiles.

Effect of thermal radiation parameter (R) on the temperature profile where the horizontal axis denotes the radial position (r), while the vertical axis corresponds to the temperature component (θ_0).

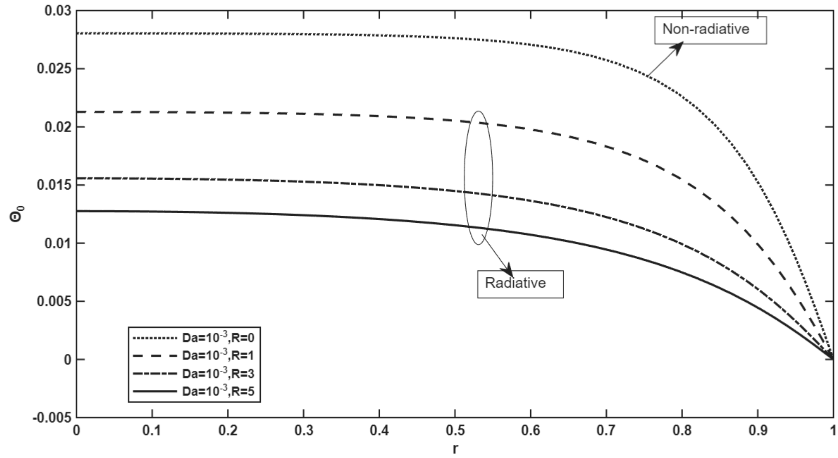

Figure 8: Temperature profile $Da = 10^{-3}$.

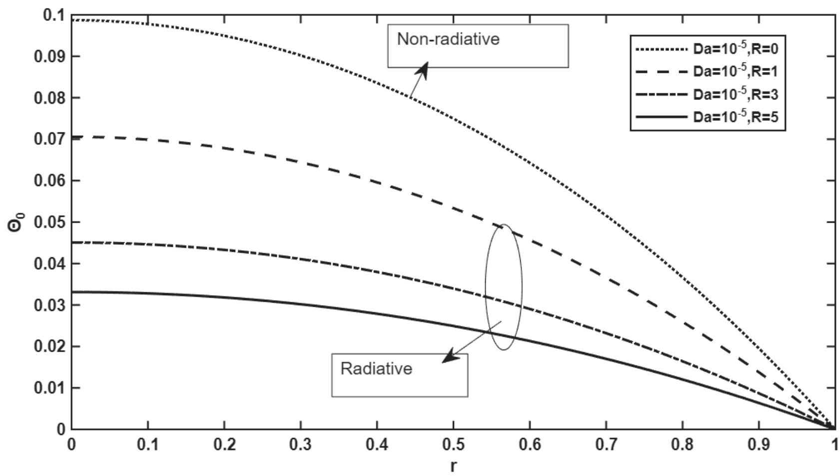

Figure 9: Temperature profile $Da = 10^{-5}$.

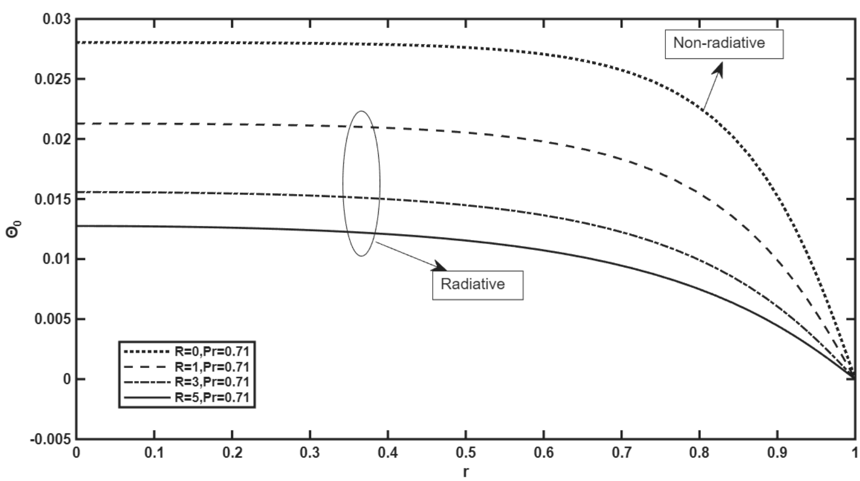

Figure 10: Temperature profile for $Pr = 0.71$.

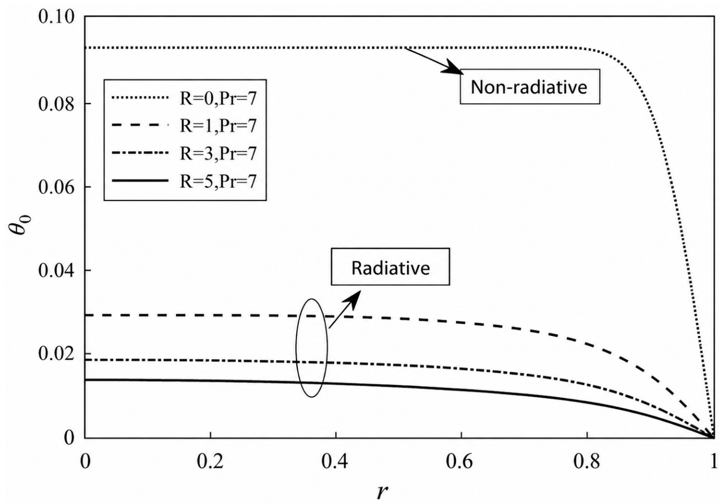

Figure 11: Temperature profile for $Pr = 7$.

Figures 10 and 11 indicate the impact of the R on the temperature profiles of air and water, respectively. These graphs show, increasing the radiation parameter produces a drop in the temperature of both air and water. Effect of radiation parameter(R) is more pronounced in case of water as compare to air. This difference arises from the higher Prandtl number of water, which implies lower thermal diffusivity relative to momentum diffusivity. As a result, heat diffuses more slowly, forming a thinner thermal boundary layer and reducing the core fluid temperature. In contrast, air's lower Prandtl number allows faster heat diffusion, producing a thicker boundary layer and a milder temperature drop with radiation. Similar kind of phenomenon observed by Mwamba et al. [18] analyzing hydromagnetic flow in a cylinder subjected to thermal radiation and chemical reaction effects.

4.4 Concentration profile

Figures 12 and 13 represents effect of radiation parameter on concentration distribution for Darcy value $Da = 10^{-3}$ and $Da = 10^{-5}$ accordingly. The figures indicate that as the radiation parameter increases from 1 to 3 and then to 5, a clear rise in the concentration profile is observed. This behavior is attributed to the fact that radiative energy enhances thermal agitation, promoting greater molecular motion and diffusion of solute particles. The increased energy supply reduces solutal stratification, resulting more concentration distribution. Similar observation seen in Krishnamurty et al. [14]. In their experiment, they investigated the influence of chemical reactions and heat transfer on the flow of the MHD boundary layer within a porous medium.

Figures 14 and 15 represents the effect of γ on the concentration profiles of air and water respectively. As γ increases, the concentration profile consistently decreases in both cases. This decline is attributed to the enhanced rate of chemical reaction, which consumes the solute species more rapidly, thereby lowering the solute concentration. From a physical standpoint, a higher γ signifies a stronger reaction rate, acting as a sink in the species transport equation. This reduces molecular diffusivity and limits solute spreading. The effect is more noticeable in water due to its higher Schmidt number, indicating lower mass diffusivity and greater suppression of concentration under reactive conditions. This decreasing trend of chemical reaction parameter towards concentration profile also observed in [33, 10].

Figure 16 and 17 represents the impact of Sc on concentration distribution for air and water separately. A particular case is discussed taking the fluid at 25°. Figure 16 plotted for air (Pr $= 0.71$), considering Methane CH_4; Sc $= 0.99$, Oxygen O_2; Sc $= 0.84$, Carbon dioxide Co_2; Sc $= 1.14$ and Ammonia NH_3; Sc $= 0.57$, as provided in [13] and it has been seen that Sc has a decreasing trend towards concentration. Figure 17 represents concentration distribution for water (Pr $= 7$) under consideration of Sc values, Methane CH_4; Sc $= 570$, Oxygen O_2; Sc $= 441$, Carbon dioxide Co_2; Sc $= 410$ and Ammonia NH_3; Sc $= 360$ [13]. Figure 17 clearly shows that with a rise in Schmidt number concentration profile decreases, similar observation found in [18]. This happens due to the rising Schmidt number, which suggests mass transmission is less effective than the momentum transfer. As mass diffusion diminishes, so does the concentration distribution. The momentum diffusivity in the pipe's core is greater than that towards the wall.

Thermal radiation parameter (R), chemical reaction(γ) and Schmidt number(Sc) effect on concentration profile where the horizontal axis denotes the radial position (r), while the vertical axis corresponds to the concentration component (Φ_0).

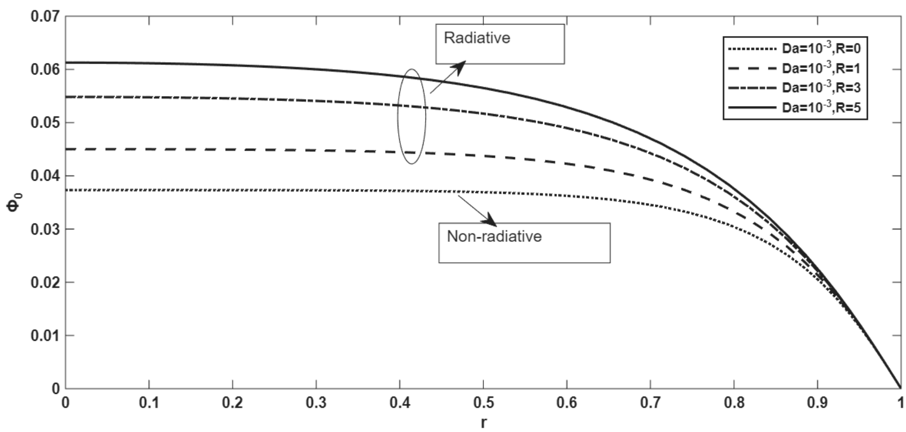

Figure 12: Concentration profile for $Da = 10^{-3}$.

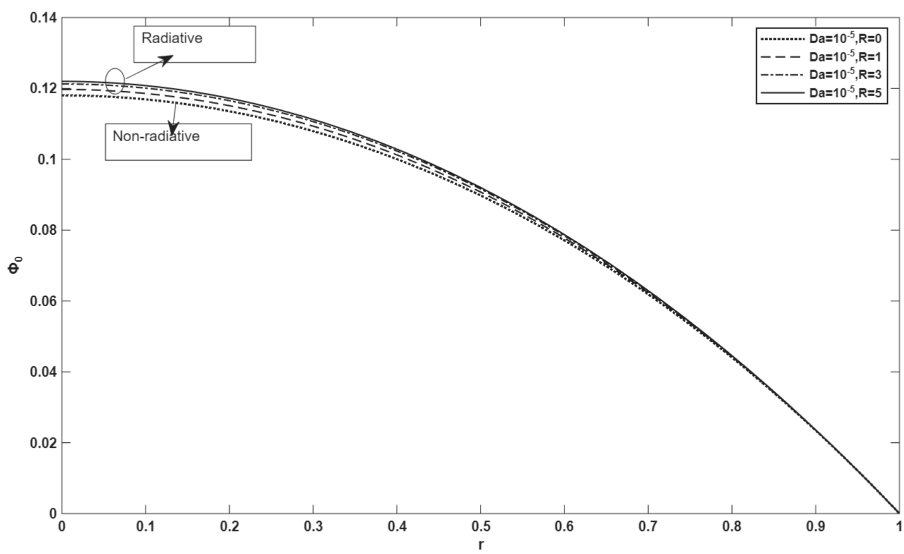

Figure 13: Concentration profile for $Da = 10^{-5}$.

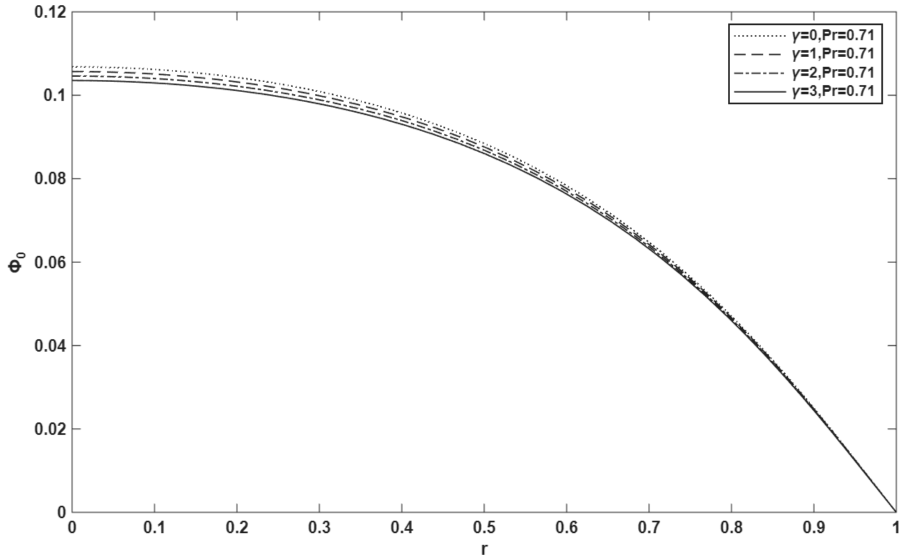

Figure 14: Concentration profile for $Pr = 0.71$.

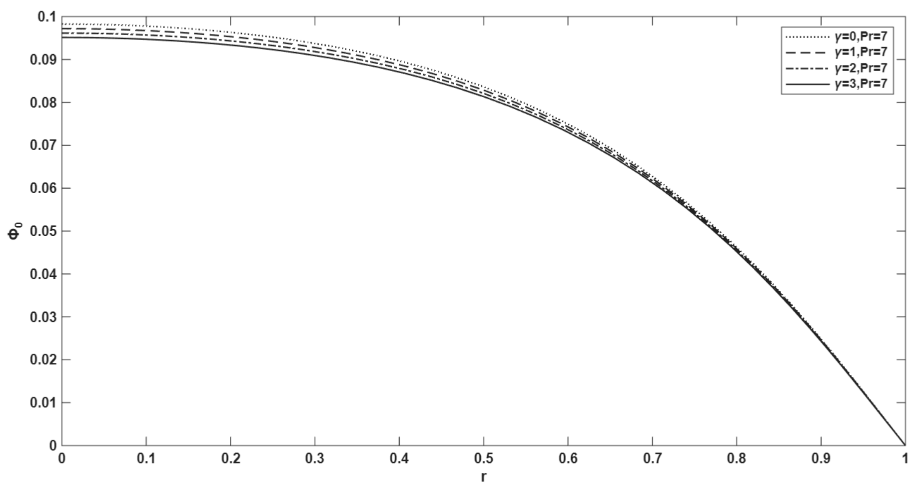

Figure 15: Concentration profile for $Pr = 7$.

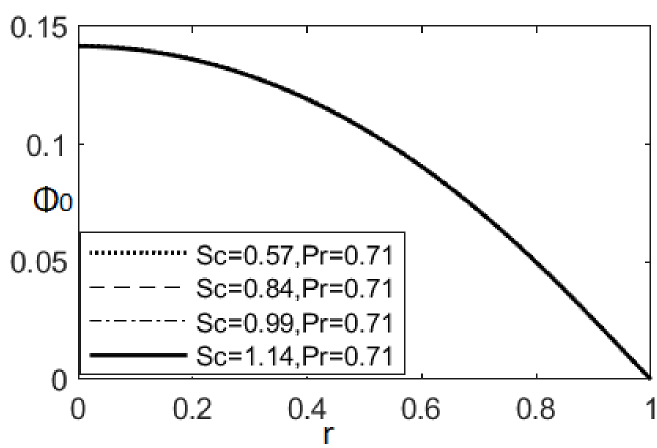

Figure 16: Concentration profile for different values of Sc and $Pr = 0.71$.

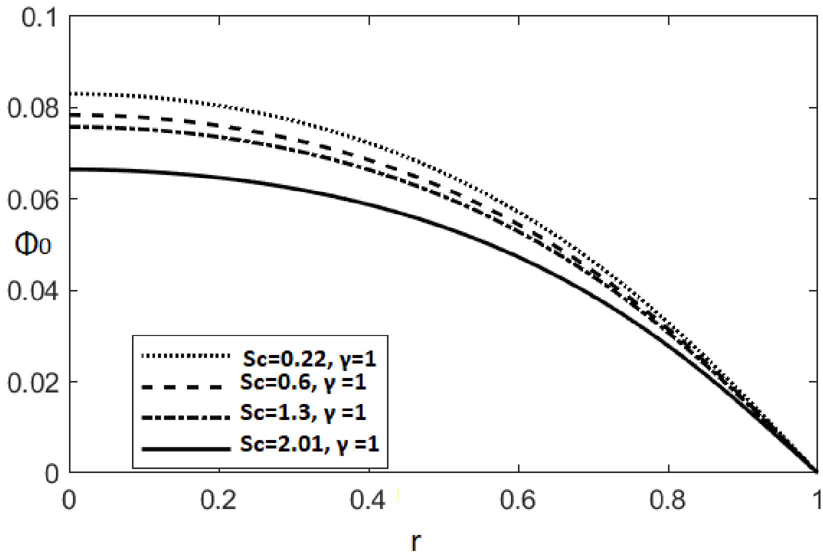

Figure 17: Concentration profile for different values of Sc and $Pr = 7$.

5 Conclusions

The study investigated thermal radiation (R) and chemical reaction (γ) effects on fully developed thermosolutal mixed convection in a vertical pipe filled with a porous medium.The proposed model is applicable to systems like high-temperature reactors, solar thermal collectors, and waste heat recovery units, where radiative heat transfer in vertical porous media is significant. It also applies to catalytic reactors and biomedical implants, where chemical reactions are influenced by temperature and concentration gradients.The flow behavior is modeled using the non-Darcy Brinkman-Forchheimer (NDBF) formulation. The resulting one-dimensional, fully developed, and coupled governing equations are solved numerically using the Chebyshev spectral collocation method. We validated our numerical results in two ways: first, by assessing the solution's sensitivity to grid size variations in the Chebyshev polynomial order and second, by confirming strong agreement between our results and established benchmark solutions under limiting conditions. Basically, the research is conducted to find the effect of thermal radiation (R) and chemical reaction (γ) on the flow mechanism in the pipe filled with porous medium for air and water system. Also the impact of Darcy number (Da) with a variation 10^{-2}, 10^{-3}, 10^{-4} and 10^{-5} on flow mechanism and effect of Schmidt number on concentration profile are explored.

1. With a variation of Darcy value (Da), 10^{-2}, 10^{-3}, 10^{-4} and 10^{-5} the velocity profile posses point of inflection and with a decreasing Darcy from 10^{-2} to 10^{-5} value the pint of inflection moves towards the wall. It has also been identified that the radiation impact causes such points of inflection to occur quickly. Radiation parameter, R enhance the instability in fluid flow mechanism.

2. For air and water, in a Darcy porous medium with Darcy value 10^{-3}, the velocity profile decreases as the radiation parameter, R increases from 1 to 3 and finally to 5.

3. Radiation parameter, R has decreasing trend towards temperature profile and the temperature is highest at the center and declines towards the wall of the pipe.

4. The temperature distribution for air, $\Pr = 0.71$ and water, $\Pr = 7$ falls with a rise in R from 1 to 3 and then to 5. The consequences of radiation parameter, R is more prominent in case of water as compare to air.

5. The concentration distribution for mixed convective flow, using two Darcy values 10^{-3} and 10^{-3}, grows as R grows from 1 to 3 and eventually to 5.

6. Effect of γ on concentration profile for air and water is perceived as, concentration profile falls with growth in chemical reaction parameter γ in a range between 1 to 3.

7. As a higher Schmidt number reduces mass diffusion, results a decrease in concentration distribution. Similar phenomenon observed here for air-water system at 25° considering Methane CH_4, Oxygen O_2, Carbon dioxide Co_2 and Ammonia NH_3.

The present study, while offering valuable insights, has certain limitations that open avenues for future research. This study is limited to steady, laminar, and fully developed vertical pipe flow with homogeneous, isotropic porous media. It uses a first-order chemical reaction and the Rosseland approximation for radiation, which may not apply to all scenarios. Future work may address transient or turbulent flows, anisotropic media, complex reaction kinetics, more general radiation models, and extended geometries for broader applicability.

Acknowledgement The authors acknowledge the financial support received through the MRIP Fellowship (Letter No. 1357/240/OSHEC) provided by the Government of Odisha.

Conflicts of Interest The authors have no conflict of interest.

References

[1] F. Ahmad, M. Nazeer, M. Saeed, A. Saleem & W. Ali (2020). Heat and mass transfer of temperature-dependent viscosity models in a pipe: Effects of thermal radiation and heat generation. *Zeitschrift für Naturforschung A*, *75*(3), 225–239. https://doi.org/10.1515/zna-2019-0332.

[2] F. Akter, M. M. Islam, A. Islam, M. S. Khan & M. S. Hossain (2016). Chemical reaction and thermal diffusion effects on mass transfer flow through an inclined plate. *Open Journal of Fluid Dynamics*, *6*(1), 62–74. https://doi.org/10.4236/ojfd.2016.61006.

[3] S. M. Arifuzzaman, M. S. Khan, M. S. Islam, M. M. Islam, B. M. J. Rana, P. Biswas & S. F. Ahmmed (2017). MHD Maxwell fluid flow in presence of nano-particle through a vertical porous-plate with heat-generation, radiation absorption and chemical reaction. *Frontiers in Heat and Mass Transfer*, *9*, Article ID: 25. https://doi.org/10.5098/hmt.9.25.

[4] N. Bachok, A. Ishak & I. Pop (2011). On the stagnation-point flow towards a stretching sheet with homogeneous–heterogeneous reactions effects. *Communications in Nonlinear Science and Numerical Simulation*, *16*(11), 4296–4302. https://doi.org/10.1016/j.cnsns.2011.01.008.

[5] P. Bera, S. Kapoor & M. K. Khandelwal (2012). Double-diffusive mixed convection in a vertical pipe: A thermal non-equilibrium approach. *International Journal of Heat and Mass Transfer*, *55*(23–24), 7079–7092. https://doi.org/10.1016/j.ijheatmasstransfer.2012.07.022.

[6] A. Campo & C. Schuler (1988). Thermal radiation and laminar forced convection in a gas pipe flow. *Wärme-und Stoffübertragung*, *22*(5), 251–257. https://doi.org/10.1007/BF01377250.

[7] J. Chiou (1993). Combined radiation-convection heat transfer in a pipe. *Journal of Thermophysics and Heat Transfer*, *7*(1), 178–180. https://doi.org/10.2514/3.11589.

[8] M. Chitra & V. Kavitha (2020). Effect of chemical reaction on MHD flow of fluid through a vertical pipe filled with porous medium. In *AIP Conference Proceedings*, volume 2261 pp. Article ID: 030019. AIP Publishing LLC, New York, United States. https://doi.org/10.1063/5.0017106.

[9] T. Hayat, M. Mustafa & S. Asghar (2010). Unsteady flow with heat and mass transfer of a third grade fluid over a stretching surface in the presence of chemical reaction. *Nonlinear Analysis: Real World Applications*, *11*(4), 3186–3197. https://doi.org/10.1016/j.nonrwa.2009.11.012.

[10] T. Hayat, T. Muhammad, S. A. Shehzad, A. Alsaedi & F. Al-Solamy (2016). Radiative three-dimensional flow with chemical reaction. *International Journal of Chemical Reactor Engineering*, *14*(1), 79–91. https://doi.org/10.1515/ijcre-2014-0179.

[11] S. Kapoor, P. Bera & A. Kumar (2012). Effect of Rayleigh thermal number in double diffusive non-Darcy mixed convective flow in vertical pipe filled with porous medium. *Procedia Engineering*, *38*, 314–320. https://doi.org/10.1016/j.proeng.2012.06.040.

[12] H. P. Kok, E. N. K. Cressman, W. Ceelen, C. L. Brace, R. Ivkov, H. Grüll, G. Ter Haar, P. Wust & J. Crezee (2020). Heating technology for malignant tumors: A review. *International Journal of Hyperthermia*, *37*(1), 711–741. https://doi.org/10.1080/02656736.2020.1779357.

[13] V. F. Krapivin & J. J. Kelley (2009). *Global Climatology and Ecodynamics: Anthropogenic Changes to Planet Earth*, chapter Model-based method for the assessment of global change in the nature-society system, pp. 133–183. Springer, Berlin, Heidelberg. https://doi.org/10.1007/978-3-540-78209-4_7.

[14] M. R. Krishnamurthy, B. C. Prasannakumara, B. J. Gireesha & R. S. R. Gorla (2016). Effect of chemical reaction on MHD boundary layer flow and melting heat transfer of Williamson nanofluid in porous medium. *Engineering Science and Technology, an International Journal*, *19*(1), 53–61. https://doi.org/10.1016/j.jestch.2015.06.010.

[15] A. Kumar, P. Bera & J. Kumar (2011). Non-Darcy mixed convection in a vertical pipe filled with porous medium. *International Journal of Thermal Sciences*, *50*(5), 725–735. https://doi.org/10.1016/j.ijthermalsci.2010.11.018.

[16] M. R. Madhavi, W. Sridhar & P. Nagesh (2021). Numerical investigations of MHD Casson nanofluid flow over a wedge through porous medium. In *AIP Conference Proceedings*, volume 2375 pp. Article ID: 030011. AIP Publishing LLC, New York, USA. https://doi.org/10.1063/5.0066944.

[17] P. M. Matao, B. P. Reddy & J. M. Sunzu (2024). Hall and viscous dissipation effects on mixed convective MHD heat absorbing flow due to an impulsively moving vertical porous plate with ramped surface temperature and concentration. *ZAMM-Journal of Applied Mathematics and Mechanics/Zeitschrift für Angewandte Mathematik und Mechanik*, *104*(5), Article ID: e202300210. https://doi.org/10.1002/zamm.202300210.

[18] N. Mwamba, J. Okelo Abonyo & K. O. Awuor (2023). Effects of thermal radiation and chemical reaction on hydromagnetic fluid flow in a cylindrical collapsible tube with an obstacle. *International Journal of Mathematics and Mathematical Sciences*, *2023*(1), Article ID: 9991376. https://doi.org/10.1155/2023/9991376.

[19] N. J. Noon (2025). Rotating thermosolutal convection for the Darcy-Brinkman model with variable gravity and chemical reaction influences. *Malaysian Journal of Mathematical Sciences*, *19*(2), 595–611. https://doi.org/10.47836/mjms.19.2.12.

[20] G. Ooms, G. Groen, D. P. de Graag & J. F. Ballintijn (1978). On turbulent pipe flow with heat transfer and chemical reaction. *Chemical Engineering Science*, *33*(3), 357–363. https://doi.org/10.1016/0009-2509(78)80093-1.

[21] S. Rani, V. R. Reddy, W. Sridhar, A. Akgül, A. M. Alsharari & J. Asad (2024). MHD stagnation point radiative flow of hybrid Casson nanofluid across a stretching surface. *Contemporary Mathematics*, *5*(2), 1590–1605. https://doi.org/10.37256/cm.5220242770.

[22] A. Raptis (1998). Flow of a micropolar fluid past a continuously moving plate by the presence of radiation. *International Journal of Heat and Mass Transfer*, *41*(18), 2865–2866. https://doi.org/10.1016/S0017-9310(98)00006-4.

[23] B. P. Reddy (2019). Effects of chemical reaction on transient MHD flow with mass transfer past an impulsively fixed infinite vertical plate in the presence of thermal radiation. *International Journal of Applied Mechanics and Engineering*, *24*(4), 169–182. https://doi.org/10.2478/ijame-2019-0056.

[24] B. P. Reddy, A. J. Kobia & M. P. Matao (2024). Unsteady mixed convection hydro-magnetic casson thermo-diffusion flow of reacting and dissipating fluid with an inclined magnetic field along an oscillating slanted porous plate. *Computational Thermal Sciences: An International Journal*, *16*(1), 57–79. https://doi.org/10.1615/ComputThermalScien.2023050323.

[25] B. P. Reddy, O. D. Makinde & A. Hugo (2022). A computational study on diffusion-thermo and rotation effects on heat generated mixed convection flow of MHD Casson fluid past an oscillating porous plate. *International Communications in Heat and Mass Transfer*, *138*, Article ID: 106389. https://doi.org/10.1016/j.icheatmasstransfer.2022.106389.

[26] B. P. Reddy, P. M. Matao & J. M. Sunzu (2024). A finite difference study of radiative mixed convection MHD heat propagating Casson fluid past an accelerating porous plate including viscous dissipation and Joule heating effects. *Heliyon*, *10*(7), Article ID: e28591. https://doi.org/10.1016/j.heliyon.2024.e28591.

[27] B. P. Reddy & L. J. Sademaki (2022). Research article a numerical study on Newtonian heating effect on heat absorbing MHD Casson flow of dissipative fluid past an oscillating vertical porous plate. *International Journal of Mathematics and Mathematical Sciences*, *2022*(1), Article ID: 7987315. https://doi.org/10.1155/2022/7987315.

[28] B. P. Reddy, M. H. Simba & A. Hugo (2023). Effects of thermodiffusion and chemical reaction on magnetohydrodynamic-radiated unsteady flow past an exponentially accelerated inclined permeable plate embedded in a porous medium. *International Journal of Chemical Engineering*, *2023*(1), Article ID: 9342174. https://doi.org/10.1155/2023/9342174.

[29] G. Sankad & M. Dhange (2017). Effect of chemical reactions on dispersion of a solute in peristaltic motion of Newtonian fluid with wall properties. *Malaysian Journal of Mathematical Sciences*, *11*(3), 347–363.

[30] C. Schuler & A. Campo (1988). Numerical prediction of turbulent heat transfer in gas pipe flows subject to combined convection and radiation. *International Journal of Heat and Fluid Flow*, *9*(3), 308–315. https://doi.org/10.1016/0142-727X(88)90042-2.

[31] P. R. Sobhana Babu, P. Jayalakshmi, D. V. N. S. R. Murthy, C. Srinivasulu & W. Sridhar (2024). Numerical investigation of Williamson fluid in presence of chemical reaction towards a parabolic surface. *International Journal of Modelling and Simulation*, *0*(0), 1–13. https://doi.org/10.1080/02286203.2024.2441487.

[32] W. Sridhar, G. Dharmaiah, K. AL-Farhany & M. F. Al-Dawody (2024). A computational ascertainment of Hall and ion slip implications over a stretched regime with chemical reaction and internal heat source. *International Journal of Ambient Energy*, *45*(1), Article ID: 2288145. https://doi.org/10.1080/01430750.2023.2288145.

[33] S. Srinivas, A. Vijayalakshmi, A. S. Reddy & T. R. Ramamohan (2016). MHD flow of a nanofluid in an expanding or contracting porous pipe with chemical reaction and heat source/sink. *Propulsion and Power Research*, *5*(2), 134–148. https://doi.org/10.1016/j.jppr.2016.04.004.

[34] L. N. Trefethen (2000). *Spectral Methods in MATLAB*. SIAM, Philadelphia, USA. https://doi.org/10.1137/1.9780898719598.

[35] L. K. Yang (1991). Combined mixed convection and radiation in a vertical pipe. *International Communications in Heat and Mass Transfer*, *18*(4), 419–430. https://doi.org/10.1016/0735-1933(91)90058-C.

[36] L. K. Yang (1992). Forced convection in a vertical pipe with combined buoyancy and radiation effects. *International Communications in Heat and Mass Transfer*, *19*(2), 249–262. https://doi.org/10.1016/0735-1933(92)90036-H.

[37] S. R. Yedhiri, S. R. Puchakayala, K. K. Palaparthi & H. Kommaddi (2024). Consequences of thermal diffusion and chemical reaction on mixed convection MHD Casson fluid through porous media with inclined plates. *CFD Letters*, *16*(9), 64–80. https://doi.org/10.37934/cfdl.16.9.6480.